On the error estimates for the divergence-free wavelet-based projection method

Souleymane Kadri Harouna, Valérie Perrier

ON THE ERROR ESTIMATES FOR THE DIVERGENCE-FREE WAVELET-BASED PROJECTION METHOD

SOULEYMANE KADRI HAROUNA* AND VALÉRIE PERRIER†

Abstract. We investigate the stability and convergence of the divergence-free wavelet-based projection method applied to the Navier-Stokes equations. Our analysis shows that the convergence rates of velocity and pressure in the time discretization are of the same order, even when using a second order scheme. This is in contrast to conventional methods, which typically suffer a loss of a factor of 1/2 in the pressure approximation. Numerical experiments on benchmark flows validate the theoretical results and highlight the efficiency of our approach.

Key words. Projection method, Divergence-free wavelets, Navier-Stokes equations.

1. Introduction. The main challenges in developing a numerical method for approximating Navier-Stokes solutions arise from the incompressibility constraint that couples velocity and pressure. Typically, to address this constraint, two different spaces are used for the spatial discretization of the unknowns, with the aim of satisfying the Babouska-Brezzi inf-sup condition that stabilises the system [3]. However, this approach increases the numerical cost of the resulting algorithms and requires more memory storage.

The projection method initiated by Chorin and Temam [4, 9, 15] in the sixties is an approach that decouples the computation of the velocity field and the pressure. An intermediate non-incompressible velocity is computed and then projected onto the divergence-free function space. The advantage is that each step of the method requires only an elliptic problem solver. However, the projection method imposes artificial boundary conditions on the pressure. This leads to a lack of precision and accuracy in the time discretization and produces boundary oscillations, especially in the pressure approximation. It is also known that classical error estimation for high order schemes loses a factor of 1/2 in the pressure time discretization rate [8].

Recently, new constructions of divergence-free wavelet bases, satisfying physical boundary conditions [11, 14], have enabled the derivation of stable bases for the Navier-Stokes solution space. By inverting the Gram matrix of such a basis, it becomes possible to project onto the divergence function space without relying on non-physical boundary conditions [4, 9, 15]. This approach was employed in [12], where the projection step was replaced by the Helmholtz-Hodge decomposition of the intermediate velocity field. In this scenario, the resulting method closely resembles Gauge method [16]. For the velocity approximation, the convergence of the method presented in [12] has been proven using the one-order Euler scheme in time and numerically studied for the two-order Crank-Nicholson scheme. However, regarding the pressure, there has been no exploration of the convergence rate in the context of the divergence-free wavelet-based projection method.

The aim of this study is to examine the time discretization error and the stability

*Laboratoire Mathématiques, Image et Applications (MIA), Université de La Rochelle, Avenue Michel Crépeau 17042 La Rochelle, France (souleymane.kadri_harouna@univ-lr.fr).

†Univ. Grenoble Alpes, CNRS, Grenoble INP, LJK, 38000 Grenoble, France. (valerie.perrier@univ-grenoble-alpes.fr).

of the divergence-free wavelet-based projection method, particularly when employing a time discretization scheme with a minimum order of two. Specifically, the analysis will demonstrate that when using the L^2 or H^1 norm for error estimation, the convergence rate of the proposed method in time discretization for the pressure is consistent with that of the velocity field approximation. This stands in contrast to the conventional projection method or the Gauge method [8, 16]. Consequently, the conjecture 5.1 of [8] is addressed in the context of the divergence-free wavelet-based projection method.

The remainder of the paper is organized as follows. In Section 2, we revisit the primary steps of the divergence-free wavelet-based projection method and introduce the time discretization schemes that will be analyzed. Section 3 focuses on the numerical error study and convergence rate estimation. Finally, Section 5 presents numerical experiments aimed at validating the theoretical results from the preceding sections.

2. Divergence-free wavelets based projection method. Initiated by Chorin and Temam [4, 9, 15], the projection method is an operator splitting method that reduces the numerical resolution of the Navier-Stokes equations to successive elliptic problem resolutions. Due to its simplicity, it has gained widespread popularity, and several improvements have been made to the initial algorithms. Broadly, there are three types of projection method algorithms [8]: the pressure-correction method, the velocity-correction method, and the consistent splitting method. The divergence-free wavelet-based method falls under the category of consistent splitting methods. In this section, we revisit its main steps, as outlined in [12], particularly when utilizing the Crank-Nicholson scheme or the Gear scheme, both of which are second-order time discretization schemes.

As we are dealing with an operator splitting method, our focus will be on the linear equations. It is worth noting that the non-linear term can be discretized in a manner that does not impact this error. Specifically, let $\Omega \subset \mathbb{R}^d$ ($d = 2$ or $d = 3$) be an open bounded set with a "smooth" boundary $\partial\Omega$. Without loss of generality, we consider the unsteady incompressible Stokes equations in the primitive variables formulation:

$$\begin{cases} \partial_t \boldsymbol{v} - \nu\Delta\boldsymbol{v} + \nabla p = \boldsymbol{f}, \text{ in } \Omega \times [0,T], \\ \nabla \cdot \boldsymbol{v} = 0 \text{ in } \Omega \times [0,T], \\ \boldsymbol{v}_{|\partial\Omega} = 0 \text{ in } [0,T],\ \boldsymbol{v}(0,x) = \boldsymbol{v}_0 \text{ in } \Omega, \end{cases} \tag{2.1}$$

where $\boldsymbol{f}$ is a source term and $\boldsymbol{v}_0$ is a divergence-free vector field. Both are assumed to be sufficiently "smooth" concerning their arguments. The unknowns in system (2.1) are the velocity vector field $\boldsymbol{v}$ and the pressure scalar field p.

The time numerical discretization of (2.1) is obtained using finite difference methods. Then, given a time step $\delta t > 0$, we set $\boldsymbol{v}^0(x) = \boldsymbol{v}_0(x)$ and denote by $\boldsymbol{v}^n(x)$ the approximation of $v(x, n\delta t)$ for an integer $n \geq 1$: $\boldsymbol{v}^n(x) \approx \boldsymbol{v}(x, n\delta t)$. In the works of the literature, the most common second-order schemes used to compute $\boldsymbol{v}^n(x)$ are the Crank-Nicholson scheme and the Gear scheme, which we have summarized as fallows:

- Crank-Nicholson's scheme:

$$\begin{cases} \frac{\boldsymbol{v}^{n+1}-\boldsymbol{v}^n}{\delta t} - \frac{\nu}{2}\Delta(\boldsymbol{v}^{n+1}+\boldsymbol{v}^n) + \frac{1}{2}\nabla(p^{n+1}+p^n) = \frac{1}{2}(\boldsymbol{f}^{n+1}+\boldsymbol{f}^n), \\ \nabla\cdot\boldsymbol{v}^n = 0, \\ \boldsymbol{v}^n = 0 \ \text{ on } \ \partial\Omega. \end{cases} \tag{2.2}$$

- Gear scheme:

$$\begin{cases} \frac{3\boldsymbol{v}^{n+1}-4\boldsymbol{v}^n+\boldsymbol{v}^{n-1}}{2\delta t} - \nu\Delta\boldsymbol{v}^{n+1} + \nabla p^{n+1} = \boldsymbol{f}^{n+1}, \\ \nabla\cdot\boldsymbol{v}^n = 0, \\ \boldsymbol{v}^n = 0 \ \text{ on } \ \partial\Omega. \end{cases} \tag{2.3}$$

Then, following [12], the divergence-free wavelet-based time discretization associated with the Crank-Nicholson scheme (2.2) reads:

$$\begin{cases} \frac{\tilde{\boldsymbol{v}}^{n+1}-\boldsymbol{v}^n}{\delta t} - \frac{\nu}{2}\Delta(\tilde{\boldsymbol{v}}^{n+1}+\boldsymbol{v}^n) &=& \frac{1}{2}(\boldsymbol{f}^{n+1}+\boldsymbol{f}^n), \\ \boldsymbol{v}^{n+1} = \mathbb{P}^{div,0}(\tilde{\boldsymbol{v}}^{n+1}). \end{cases} \tag{2.4}$$

Similarly, for the Gear scheme (2.3), we have:

$$\begin{cases} \frac{3\tilde{\boldsymbol{v}}^{n+1}-4\boldsymbol{v}^n+\boldsymbol{v}^{n-1}}{2\delta t} - \nu\Delta(\tilde{\boldsymbol{v}}^{n+1}) &=& \boldsymbol{f}^{n+1}, \\ \boldsymbol{v}^{n+1} = \mathbb{P}^{div,0}(\tilde{\boldsymbol{v}}^{n+1}). \end{cases} \tag{2.5}$$

In (2.4) and (2.5), $\mathbb{P}^{div,0}$ refers to the orthogonal projector onto the divergence-free function subspace of $H_0^1(\Omega)^d$. The intermediate velocity $\tilde{\boldsymbol{v}}^{n+1}$ is defined as:

$$\tilde{\boldsymbol{v}}^{n+1} = \boldsymbol{v}^{n+1} + \nabla\Phi^{n+1}, \tag{2.6}$$

where Φ^{n+1} is a *regular* scalar field defined on Ω that comes from the Helmholtz-Hodge decomposition of $\tilde{\boldsymbol{v}}^{n+1}$.

Remark 2.1.
The numerical solutions of (2.2) *and* (2.3) *and the solutions of* (2.4) *and* (2.5) *are denoted here by* $\boldsymbol{v}^{n+1}$ *to simplify the notation and avoid redundancy. There's no a priori reason why they should be the same.*

In view of (2.4) and (2.5), a major difficulty is to obtain consistency of the operator splitting. To illustrate this point, let us replace $\tilde{\boldsymbol{v}}^{n+1}$ with its expression (2.6) in the first equation of (2.4):

$$\frac{\boldsymbol{v}^{n+1}-\boldsymbol{v}^n}{\delta t} - \frac{\nu}{2}\Delta(\boldsymbol{v}^{n+1}+\boldsymbol{v}^n) + \nabla\left[\frac{1}{\delta t}\Phi^{n+1} - \frac{\nu}{2}\Delta\Phi^{n+1}\right] = \frac{1}{2}(\boldsymbol{f}^{n+1}+\boldsymbol{f}^n). \tag{2.7}$$

It can then be observed that if the pressure satisfies the following relationship

$$\frac{1}{2}(\nabla p^{n+1} + \nabla p^n) = \nabla\left[\frac{1}{\delta t}\Phi^{n+1} - \frac{\nu}{2}\Delta\Phi^{n+1}\right]. \tag{2.8}$$

Thus the formulations (2.4) and (2.5) are nothing more than a change of variables. However, when using the elliptic problem solver to compute $\boldsymbol{v}^n$, the relation (2.8) is not satisfied due to the lack of correct boundary conditions on the numerical pressure p^n and velocity $\boldsymbol{v}^n$. Furthermore, the assumption that the equality (2.8) is satisfied is at the origin of the name of the *consistent splitting method* or *change of variables method*, this is also the basis of the *gauge method* [16].

In the case of the divergence-free wavelet-based method, we argue that the relation (2.8) holds, and this will be shown in the next upcoming section. Thus, at each time step, one can define the pressure approximation using the auxiliary scalar field Φ^{n+1}. More precisely, for the Crank-Nicholson scheme, the pressure approximation is defined by

$$\nabla\bar{p}^{n+1/2} = \frac{1}{2}(\nabla\bar{p}^{n+1} + \nabla\bar{p}^n) = \nabla\left[\frac{1}{\delta t}\Phi^{n+1} - \frac{\nu}{2}\Delta\Phi^{n+1}\right], \tag{2.9}$$

and similarly for the Gear system:

$$\nabla\bar{p}^{n+1} = \nabla\left[\frac{3}{2\delta t}\Phi^{n+1} - \nu\Delta\Phi^{n+1}\right]. \tag{2.10}$$

A key objective of this study is to demonstrate that the numerical pressure $\bar{p}^n$, defined by (2.9) and (2.10), obtained by replacing $\tilde{\boldsymbol{v}}^{n+1}$ with (2.6) in (2.4) and (2.5) respectively, approximates the exact pressure $p(t^n)$ with a time discretization rate of approximately $\mathcal{O}(\delta t^2)$. This aligns with the expected rate of discretization for $\boldsymbol{v}(x, n\delta t)$ and $\nabla\boldsymbol{v}(x, n\delta t)$ in the L^2-norm, as provided by schemes (2.2) and (2.3).

3. Estimates on the time discretization error . Despite the large literature on the projection method, even today, its major drawback is that the estimation of the time discretization error on the pressure and velocity gradient is not optimal for schemes of two order and higher. Although numerical experiments show the expected order in certain situations [5, 8]. In this section we delve into the time discretization error of the divergence-free wavelet-based schemes (2.4) and (2.5). To avoid redundancy, we will concentrate on the Crank-Nicholson scheme (2.4). For the Gear scheme (2.5), we will outline the crucial steps and corresponding estimates. Then, assuming the exact solution $(\boldsymbol{v}, p)$ and the source term $\boldsymbol{f}$ to be "smooth" enough, the numerical errors we are interested in are:

$$\boldsymbol{e}^n = \boldsymbol{v}(t^n) - \boldsymbol{v}^n \qquad \text{and} \qquad q^n = p(t^n) - p^n, \tag{3.1}$$

where $\boldsymbol{v}^n$ is the solution of (2.2) or (2.3), without distinction. In this case, the Taylor expansion of the solution around $t^n = n\delta t$ gives:

$$\boldsymbol{v}(t^{n+1}) = \boldsymbol{v}(t^n) + \delta t\partial_t\boldsymbol{v}(t^n) + \frac{\delta t^2}{2!}\partial_t^2\boldsymbol{v}(t^n) + \frac{\delta t^3}{3!}\partial_t^3\boldsymbol{v}(t^n) + \mathcal{O}(\delta t^4),$$

and

$$\nabla p(t^{n+1}) = \nabla[p(t^n) + \delta t\partial_t p(t^n) + \frac{\delta t^2}{2!}\partial_t^2 p(t^n) + \frac{\delta t^3}{3!}\partial_t^3 p(t^n) + \mathcal{O}(\delta t^4)],$$

and

$$\boldsymbol{f}(t^{n+1}) = \boldsymbol{f}(t^n) + \delta t\partial_t\boldsymbol{f}(t^n) + \frac{\delta t^2}{2!}\partial_t^2\boldsymbol{f}(t^n) + \frac{\delta t^3}{3!}\partial_t^3\boldsymbol{f}(t^n) + \mathcal{O}(\delta t^4).$$

Thus, replacing $\boldsymbol{v}^n$ by $\boldsymbol{v}(t^n)$ in (2.4), we get:

$$\frac{\boldsymbol{v}(t^{n+1})-\boldsymbol{v}(t^n)}{\delta t}-\frac{\nu}{2}\Delta[\boldsymbol{v}(t^{n+1})+\boldsymbol{v}(t^n)]+\frac{1}{2}\left(\nabla p(t^{n+1})+\nabla p(t^n)\right)-\frac{1}{2}\left(\boldsymbol{f}(t^{n+1})+\boldsymbol{f}(t^n)\right)=$$
$$[\partial_t\boldsymbol{v}(t^n)-\nu\Delta\boldsymbol{v}(t^n)+\nabla p(t^n)-\boldsymbol{f}(t^n)]+\frac{\delta t}{2}\partial_t[\partial_t\boldsymbol{v}(t^n)-\nu\Delta\boldsymbol{v}(t^n)+\nabla p(t^n)-\boldsymbol{f}(t^n)]+$$
$$\frac{\delta t^2}{4}\partial_t^2[\partial_t\boldsymbol{v}(t^n)-\nu\Delta\boldsymbol{v}(t^n)+\nabla p(t^n)-\boldsymbol{f}(t^n)]=R_n(\delta t)+\mathcal{O}(\delta t^3), \tag{3.2}$$

where:

$$R_n(\delta t)=-\frac{\delta t^2}{12}\partial_t^3\boldsymbol{v}(t^n)=\mathcal{O}(\delta t^2).$$

Either by making the difference of (2.4) with (3.2), we deduce that:

$$\frac{\boldsymbol{e}^{n+1}-\boldsymbol{e}^n}{\delta t}-\frac{\nu}{2}\Delta[\boldsymbol{e}^{n+1}+\boldsymbol{e}^n]+\frac{1}{2}(\nabla q^{n+1}+\nabla q^n)=\mathcal{O}(\delta t^2), \tag{3.3}$$

and

$$\nabla\cdot\boldsymbol{e}^n=0 \qquad \text{and} \qquad \boldsymbol{e}^n=0 \ \text{ on } \ \partial\Omega, \ \ \forall\ n\geq 0. \tag{3.4}$$

Accordingly, the splitting errors are:

$$\tilde{\boldsymbol{e}}^n=\boldsymbol{v}(t^n)-\tilde{\boldsymbol{v}}^n=\boldsymbol{v}(t^n)-(\boldsymbol{v}^n+\nabla\Phi^n)=\boldsymbol{e}^n-\nabla\Phi^n \qquad \text{and} \qquad \bar{q}^n=q^n-\bar{p}^n, \tag{3.5}$$

where $\bar{p}$ is defined in (2.9) and (2.10), depending on the scheme considered. From (3.3), we see that:

$$\frac{\tilde{\boldsymbol{e}}^{n+1}-\boldsymbol{e}^n}{\delta t}-\frac{\nu}{2}\Delta[\tilde{\boldsymbol{e}}^{n+1}+\boldsymbol{e}^n]+\frac{1}{2}\left(\nabla\bar{q}^{n+1}+\nabla\bar{q}^n\right)=\mathcal{O}(\delta t^2). \tag{3.6}$$

It is important to note that this error is not divergence-free $\nabla\cdot\tilde{\boldsymbol{e}}^n\neq 0$, but it satisfies the Dirichlet homogeneous boundary condition as $\boldsymbol{e}^n$.

Similarly, using the previous Taylors expansion terms, the troncation error and the splitting error of the Gear scheme (2.3), denoted again by $\boldsymbol{e}^n$ and $\tilde{\boldsymbol{e}}^n$ respectively, satisfy:

$$\frac{3\boldsymbol{e}^{n+1}-4\boldsymbol{e}^n+\boldsymbol{e}^{n-1}}{2\delta t}-\nu\Delta\boldsymbol{e}^{n+1}+\nabla q^{n+1}=\mathcal{O}(\delta t^2), \tag{3.7}$$

and

$$\frac{3\tilde{\boldsymbol{e}}^{n+1}-4\boldsymbol{e}^n+\boldsymbol{e}^{n-1}}{2\delta t}-\nu\Delta\tilde{e}^{n+1}+\nabla\bar{q}^{n+1}=\mathcal{O}(\delta t^2). \tag{3.8}$$

To see the rate of decay of these errors with respect to the time step δt, we estimate their L^2 norm from equations (3.3) and (3.7).

3.1. Time discretization error. The expected time discretization convergence rate of the divergence-free wavelet-based methods (2.4) and (2.5) is in $\mathcal{O}(\delta t^2)$. To the best of our knowledge, when using numerical schemes (2.2) or (2.3), there are no works that prove the convergence of the conventional projection method with a rate $\mathcal{O}(\delta t^2)$ in pressure and velocity gradient discretization, see [8] for the discussion. The aim of this section is to study the rate of convergence of the schemes (2.4) and (2.5). We will show that the method converges in $\mathcal{O}(\delta t^2)$ in the approximation of the velocity $\boldsymbol{v}$, the velocity gradient $\nabla \boldsymbol{v}$ and the pressure p.

First, we emphasize that the numerical schemes (2.4) and (2.5) are consistent with the systems (2.2) and (2.3), respectively.

LEMMA 3.1.
Let $\boldsymbol{v}^{n+1}$ be the solution of (2.2) *or* (2.3) *and let $\bar{\boldsymbol{v}}^{n+1}$ be the solution of* (2.4) *or* (2.5). *Then, we have:*

$$\boldsymbol{v}^{n+1} = \bar{\boldsymbol{v}}^{n+1} = \mathbb{P}^{div,0}(\tilde{\boldsymbol{v}}^{n+1}). \tag{3.9}$$

Proof. We suppose that $\boldsymbol{v}^{n+1} \neq \mathbb{P}^{div,0}(\tilde{\boldsymbol{v}}^{n+1})$ and denote the difference by:

$$\boldsymbol{u}^{n+1} = \boldsymbol{v}^{n+1} - \mathbb{P}^{div,0}(\tilde{\boldsymbol{v}}^{n+1}).$$

Then, if we make the subtraction of the first equation from (2.2) and (2.4), we get

$$\frac{\boldsymbol{u}^{n+1}}{\delta t} - \frac{\nu}{2}\Delta \boldsymbol{u}^{n+1} + \frac{1}{2}(\nabla p^{n+1} + \nabla p^{n}) = 0. \tag{3.10}$$

Since we have $\nabla \cdot \boldsymbol{u}^{n+1} = 0$ and $\boldsymbol{u}^{n+1}_{|\partial\Omega} = 0$, taking the inner product of (3.10) with $\boldsymbol{u}^{n+1}$, we obtain:

$$\|\boldsymbol{u}^{n+1}\|^2_{L^2(\Omega)^d} + \frac{\delta t \nu}{2}\|\nabla \boldsymbol{u}^{n+1}\|^2_{L^2(\Omega)^{d\times d}} = 0. \tag{3.11}$$

Hence

$$\|\boldsymbol{u}^{n+1}\|^2_{L^2(\Omega)^d} = 0 \qquad \text{and} \qquad \|\nabla \boldsymbol{u}^{n+1}\|^2_{L^2(\Omega)^{d\times d}} = 0, \tag{3.12}$$

which means that $\boldsymbol{v}^{n+1} = \mathbb{P}^{div,0}(\tilde{\boldsymbol{v}}^{n+1})$ in the case of the Crank-Nicholson scheme (2.4) and the relation (2.8) is satisfied for the corresponding divergence-free wavelet-based method.

In the same way, using the same notation as before, we obtain the difference of the first equations of the systems (2.3) and (2.5):

$$\frac{3\boldsymbol{u}^{n+1}}{2\delta t} - \nu\Delta \boldsymbol{u}^{n+1} + \nabla p^{n+1} = 0. \tag{3.13}$$

Again, taking the inner product of (3.13) with $\boldsymbol{u}^{n+1}$ leads to:

$$3\|\boldsymbol{u}^{n+1}\|^2_{L^2(\Omega)^d} + 2\delta t\nu\|\nabla \boldsymbol{u}^{n+1}\|^2_{L^2(\Omega)^{d\times d}} = 0. \tag{3.14}$$

Thus:

$$\|\boldsymbol{u}^{n+1}\|^2_{L^2(\Omega)^d} = 0 \qquad \text{and} \qquad \|\nabla \boldsymbol{u}^{n+1}\|^2_{L^2(\Omega)^{d\times d}} = 0, \tag{3.15}$$

which means that we have $\boldsymbol{v}^{n+1} = \mathbb{P}^{div,0}(\tilde{\boldsymbol{v}}^{n+1})$ and the projection of the intermediate velocity $\tilde{\boldsymbol{v}}^{n+1}$ is the solution of (2.5) in the case of Gear scheme. □

The theorem below outlines our principal results concerning the convergence rate of the time discretization error for the numerical schemes defined by (2.4) and (2.5):

THEOREM 3.2.
Assuming that the solution $(\boldsymbol{v}, p)$ *of* (2.1) *and the source term* $\boldsymbol{f}$ *are smooth enough in space and time. Under the initialization assumptions*

$$\|e^0\|_{L^2(\Omega)^d} + \|\nabla e^0\|_{L^2(\Omega)^{d\times d}} \leq C\delta t^2, \tag{3.16}$$

the solution $\boldsymbol{v}^n$ *of* (2.4) *satisfies:*

$$\forall\ n \geq 0, \quad \|\boldsymbol{v}^n - \boldsymbol{v}(n\delta t)\|_{L^2(\Omega)^d} + \|\nabla \boldsymbol{v}^n - \nabla \boldsymbol{v}(n\delta t)\|_{L^2(\Omega)^d} \leq C\delta t^2, \tag{3.17}$$

and

$$\forall\ n \geq 0, \ \ \|p(t^{n+1/2}) - \bar{p}^{n+1/2}\|_{L^2(\Omega)} + \|\nabla p(t^{n+1/2}) - \nabla \bar{p}^{n+1/2}\|_{H^{-1}(\Omega)^d} \leq C\delta t^2, \tag{3.18}$$

where $p(t^{n+1/2}) = \frac{1}{2}\left(p(t^{n+1}) + p(t^n)\right)$ *and* $\bar{p}^{n+1/2}$ *define in* (2.9).
Moreover, if

$$\|e^1\|_{L^2(\Omega)^d} + \|\nabla e^1\|_{L^2(\Omega)^{d\times d}} \leq C\delta t^2, \tag{3.19}$$

the solution $\boldsymbol{v}^n$ *of* (2.5) *also satisfies:*

$$\forall\ n \geq 0, \quad \|\boldsymbol{v}^n - \boldsymbol{v}(n\delta t)\|_{L^2(\Omega)^d} + \|\nabla \boldsymbol{v}^n - \nabla \boldsymbol{v}(n\delta t)\|_{L^2(\Omega)^d} \leq C\delta t^2, \tag{3.20}$$

and

$$\forall\ n \geq 0, \quad \|p(t^n) - \bar{p}^n\|_{L^2(\Omega)} + \|\nabla p(t^n) - \nabla \bar{p}^n\|_{H^{-1}(\Omega)^d} \leq C\delta t^2. \tag{3.21}$$

Proof. Let us take $\boldsymbol{e}^{n+1} + \boldsymbol{e}^n$ as the test function in (3.3). A simple calculation gives

$$\|\boldsymbol{e}^{n+1}\|^2_{L^2(\Omega)^d} - \|\boldsymbol{e}^n\|^2_{L^2(\Omega)^d} + \frac{\nu\delta t}{2}\|\nabla(\boldsymbol{e}^{n+1} + \boldsymbol{e}^n)\|^2_{L^2(\Omega)^d} \leq C\delta t^3 \|\boldsymbol{e}^{n+1} + \boldsymbol{e}^n\|_{L^2(\Omega)^d},$$

where $C > 0$ denotes a generic constant that changes from one equation to another. To bound the term $\|\nabla(\boldsymbol{e}^{n+1} + \boldsymbol{e}^n)\|^2_{L^2(\Omega)^d}$ in the previous equation, we use the Poincaré and Young's inequalities to get this:

$$\|\boldsymbol{e}^{n+1}\|^2_{L^2(\Omega)^d} - \|\boldsymbol{e}^n\|^2_{L^2(\Omega)^d} + \frac{\nu\delta t}{4}\|\nabla(\boldsymbol{e}^{n+1} + \boldsymbol{e}^n)\|^2_{L^2(\Omega)^{d\times d}} \leq \frac{C}{\nu}\delta t^5.$$

Doing an induction over n, we arrive at:

$$\|\boldsymbol{e}^n\|^2_{L^2(\Omega)^d} \leq \|\boldsymbol{e}^0\|^2_{L^2(\Omega)^d} + \frac{C}{\nu}\delta t^4.$$

Based on the assumption made on the initial condition (3.16), the first error estimate, in the L^2 norm for the velocity, is then proven for the Crank-Nicholson scheme. To

extend this to the gradient of the velocity field, a similar procedure is repeated. By employing $\boldsymbol{e}^{n+1}-\boldsymbol{e}^n$ as the test function in (3.3), the following result is obtained:

$$\begin{aligned}\|\boldsymbol{e}^{n+1}-\boldsymbol{e}^n\|^2_{L^2(\Omega)^d}+\frac{\nu\delta t}{2}\|\nabla\boldsymbol{e}^{n+1}\|^2_{L^2(\Omega)^d}-\frac{\nu\delta t}{2}\|\nabla\boldsymbol{e}^{n}\|^2_{L^2(\Omega)^d} &\leq C\delta t^3\|\boldsymbol{e}^{n+1}-\boldsymbol{e}^n\|_{L^2(\Omega)^d}\\ &\leq C\delta t^6+\frac{1}{2}\|\boldsymbol{e}^{n+1}-\boldsymbol{e}^n\|^2_{L^2(\Omega)^d}.\end{aligned}$$

If we remove the positive from the left side of the preceding inequality, we get

$$\|\nabla\boldsymbol{e}^{n+1}\|^2_{L^2(\Omega)^d}-\|\nabla\boldsymbol{e}^{n}\|^2_{L^2(\Omega)^d}\leq\frac{C}{\nu}\delta t^5,$$

and an induction over n gives:

$$\|\nabla\boldsymbol{e}^{n}\|^2_{L^2(\Omega)^d}\leq\|\nabla\boldsymbol{e}^{0}\|^2_{L^2(\Omega)^d}+\frac{C}{\nu}\delta t^4,$$

which gives the desired bound on the gradient.

To prove the pressure error estimate (3.1), we first set:

$$\nabla q^{n+1/2}=\nabla[\frac{p(t^{n+1})+p(t^n)}{2}-\frac{1}{\delta t}\Phi^{n+1}+\frac{\nu}{2}\Delta\Phi^{n+1}]=\nabla p^{n+1/2}-\nabla\bar{p}^{n+1/2},$$

where $\bar{p}^n$ is defined in (2.9), and rewrite (3.6) as:

$$\frac{\boldsymbol{e}^{n+1}-\boldsymbol{e}^n}{\delta t}-\frac{\nu}{2}\Delta[\boldsymbol{e}^{n+1}+\boldsymbol{e}^n]+\nabla q^{n+1/2}=R_n(\delta t)+\mathcal{O}(\delta t^3).\tag{3.22}$$

What is rewritten in:

$$-\frac{\nu}{2}\Delta[\boldsymbol{e}^{n+1}+\boldsymbol{e}^n]+\nabla q^{n+1/2}=\frac{\boldsymbol{e}^{n}-\boldsymbol{e}^{n+1}}{\delta t}+R_n(\delta t)+\mathcal{O}(\delta t^3)=\bar{\boldsymbol{f}}^{n+1}.\tag{3.23}$$

Since $\boldsymbol{e}^{n+1}+\boldsymbol{e}^n\in H^1_0(\Omega)^d$, the equation (3.22) can be seen as a non-homogeneous Stokes problem for the unknowns $\boldsymbol{e}^{n+1}+\boldsymbol{e}^n$ and $q^{n+1/2}$. Then classical stabilization results for the Stokes problem [6, 15] allow to get:

$$\|\boldsymbol{e}^{n+1}+\boldsymbol{e}^n\|_{H^1(\Omega)^d}+\|q^{n+1/2}\|_{L^2(\Omega)}\leq C\|\bar{\boldsymbol{f}}^{n+1}\|_{H^{-1}(\Omega)^d}.\tag{3.24}$$

Moreover, as $R_n(\delta t)=\mathcal{O}(\delta t^2)$, from (3.22) we get:

$$\begin{aligned}\|\nabla q^{n+1/2}\|_{H^{-1}(\Omega)^d} &\leq \|\frac{\boldsymbol{e}^{n+1}-\boldsymbol{e}^n}{\delta t}\|_{H^{-1}(\Omega)^d}+\frac{\nu}{2}\|\Delta[\boldsymbol{e}^{n+1}+\boldsymbol{e}^n]\|_{H^{-1}(\Omega)^d}+\mathcal{O}(\delta t^2)\\ &\leq \|\frac{\boldsymbol{e}^{n+1}-\boldsymbol{e}^n}{\delta t}\|_{H^{-1}(\Omega)^d}+\frac{\nu}{2}\|\boldsymbol{e}^{n+1}+\boldsymbol{e}^n\|_{H^1(\Omega)^d}+\mathcal{O}(\delta t^2)\end{aligned}\tag{3.25}$$

In (3.25), the term $\frac{\nu}{2}\|\boldsymbol{e}^{n+1}+\boldsymbol{e}^n\|_{H^1(\Omega)^d}$ is in $\mathcal{O}(\delta t^2)$ according to (3.17). Thus, we have:

$$\|\nabla q^{n+1/2}\|_{H^{-1}(\Omega)^d}\leq C\|\frac{\boldsymbol{e}^{n+1}-\boldsymbol{e}^n}{\delta t}\|_{L^2(\Omega)^d}+\mathcal{O}(\delta t^2).\tag{3.26}$$

To prove that $\|\frac{\boldsymbol{e}^{n+1}-\boldsymbol{e}^n}{\delta t}\|_{L^2(\Omega)^d}\leq C\delta t^2$, we will use the definition of $R_n(\delta t)$:

$$R_n(\delta t)=-\frac{\delta t^2}{12}\partial^3_t\boldsymbol{v}(t^n),$$

and calculating the increments of $R_n(\delta t)$, as done in [1], we have:

$$R_n(\delta t) - R_{n-1}(\delta t) = \delta R_n(\delta t) = \mathcal{O}(\delta t^3).$$

Then, setting $\delta \boldsymbol{e}^n = \boldsymbol{e}^n - \boldsymbol{e}^{n-1}$ and $\delta q^{n+1/2} = q^{n+1/2} - q^{n-1/2}$, from (3.22) we deduce that:

$$\frac{\delta \boldsymbol{e}^{n+1} - \delta \boldsymbol{e}^n}{\delta t} - \frac{\nu}{2}\Delta[\delta \boldsymbol{e}^{n+1} + \delta \boldsymbol{e}^n] + \nabla \delta q^{n+1/2} = \delta R_n(\delta t) = \mathcal{O}(\delta t^3). \tag{3.27}$$

Using $\delta \boldsymbol{e}^{n+1} + \delta \boldsymbol{e}^n$ as the test function in (3.27), with the help of Poincaré and Young's inequalities we have:

$$\|\delta \boldsymbol{e}^{n+1}\|^2_{L^2(\Omega)^d} - \|\delta \boldsymbol{e}^n\|^2_{L^2(\Omega)^d} + \frac{\nu \delta t}{4}\|\nabla(\delta \boldsymbol{e}^{n+1} + \delta \boldsymbol{e}^n)\|^2_{L^2(\Omega)^{d\times d}} \leq C\delta t^7.$$

Therefore, an induction over n gives:

$$\|\delta \boldsymbol{e}^{n+1}\|^2_{L^2(\Omega)^d} \leq \|\delta \boldsymbol{e}^1\|^2_{L^2(\Omega)^d} + C\delta t^6.$$

If the initialization error satisfies the following condition

$$\|\delta \boldsymbol{e}^1\|^2_{L^2(\Omega)^d} \simeq \mathcal{O}(\delta t^6), \tag{3.28}$$

what we assumed in the sequel, we have then:

$$\|\frac{\boldsymbol{e}^{n+1} - \boldsymbol{e}^n}{\delta t}\|_{L^2(\Omega)^d} \leq C\delta t^2, \quad \forall n \geq 1. \tag{3.29}$$

From (3.29) and using Sobolev's injection [6, 15], we have:

$$\|\bar{\boldsymbol{f}}^{n+1}\|_{H^{-1}(\Omega)^d} \leq C\|\bar{\boldsymbol{f}}^{n+1}\|_{L^2(\Omega)^d} \leq C\delta t^2. \tag{3.30}$$

Combining (3.24), (3.26) and (3.30), we derive that:

$$\|q^{n+1/2}\|_{L^2(\Omega)} + \|\nabla q^{n+1/2}\|_{H^{-1}(\Omega)^d} \leq C\delta t^2, \tag{3.31}$$

which is the second statement of the theorem.

For the Gear scheme (2.3), to prove the error estimate (3.20), the key ingredient is the following identity [1]:

$$\begin{aligned} 2a^{k+1}.(3a^{k+1} - 4a^k + a^{k-1}) &= |a^{k+1}|^2 + |2a^{k+1} - a^k|^2 \\ &+ |a^{k+1} - 2a^k + a^{k-1}|^2 - |a^k|^2 - |2a^k - a^{k-1}|^2, \end{aligned}$$

with $a^k \in \mathbb{R},\ k \geq 0$. Then, taking the inner product of (3.7) with $4\delta t \boldsymbol{e}^{n+1}$ and using the previous relation, we deduced that:

$$\|\boldsymbol{e}^{n+1}\|^2_{L^2(\Omega)^d} + \|2\boldsymbol{e}^{n+1} - \boldsymbol{e}^n\|^2_{L^2(\Omega)^d} - \|\boldsymbol{e}^n\|^2_{L^2(\Omega)^d} - \|2\boldsymbol{e}^n - \boldsymbol{e}^{n-1}\|^2_{L^2(\Omega)^d} \leq \frac{C}{\nu}\delta t^5,$$

and by induction we arrive at:

$$\|\boldsymbol{e}^n\|^2_{L^2(\Omega)^d} + \|2\boldsymbol{e}^n - \boldsymbol{e}^{n-1}\|^2_{L^2(\Omega)^d} \leq \|\boldsymbol{e}^0\|^2_{L^2(\Omega)^d} + \|2\boldsymbol{e}^1 - \boldsymbol{e}^0\|^2_{L^2(\Omega)^d} + \frac{C}{\nu}\delta t^4 \tag{3.32}$$

On the other hand, with $2(3\boldsymbol{e}^{n+1}-4\boldsymbol{e}^{n}+\boldsymbol{e}^{n-1})$ as the test function in (3.7), we arrive at:

$$\|\nabla\boldsymbol{e}^{n+1}\|^2_{L^2(\Omega)^{d\times d}}+\|\nabla(2\boldsymbol{e}^{n+1}-\boldsymbol{e}^{n})\|^2_{L^2(\Omega)^{d\times d}}-\|\nabla\boldsymbol{e}^{n}\|^2_{L^2(\Omega)^{d\times d}}-\|\nabla(2\boldsymbol{e}^{n}-\boldsymbol{e}^{n-1})\|^2_{L^2(\Omega)^{d\times d}}\leq\frac{C}{\nu}\delta t^5,$$

and an induction over n gives:

$$\|\nabla\boldsymbol{e}^{n}\|^2_{L^2(\Omega)^{d\times d}}+\|\nabla(2\boldsymbol{e}^{n}-\boldsymbol{e}^{n-1})\|^2_{L^2(\Omega)^{d\times d}}\leq\|\nabla\boldsymbol{e}^{0}\|^2_{L^2(\Omega)^{d\times d}}+\|\nabla(2\boldsymbol{e}^{1}-\boldsymbol{e}^{0})\|^2_{L^2(\Omega)^{d\times d}}+\frac{C}{\nu}\delta t^4 \quad (3.33)$$

Combining (3.32) and (3.33) we get (3.20). The proof of the pressure error estimate (3.21) is based on similar arguments to the proof of (3.18). Again, (3.7) is interpreted as a Stokes problem for the unknown $\boldsymbol{e}^{n+1}$ and q^{n+1}, and the most difficult part is to bound the error increments $\delta\boldsymbol{e}^n$. To do this, it is sufficient to use $4\delta t\delta\boldsymbol{e}^{n+1}$ as the test function in the equation satisfied by this increment, with the corresponding residual term $R_n(\delta t)$. This gives us

$$\|\delta\boldsymbol{e}^{n}\|^2_{L^2(\Omega)^{d}}+\|2\delta\boldsymbol{e}^{n}-\delta\boldsymbol{e}^{n-1})\|^2_{L^2(\Omega)^{d}}\leq\|\delta\boldsymbol{e}^{0}\|^2_{L^2(\Omega)^{d}}+\|2\delta\boldsymbol{e}^{1}-\delta\boldsymbol{e}^{0})\|^2_{L^2(\Omega)^{d}}+C\delta t^6,$$

which in turn gives:

$$\|\boldsymbol{e}^{n+1}-\boldsymbol{e}^{n}\|^2_{L^2(\Omega)^{d}}\leq C\delta t^6 \quad\Rightarrow\quad \|\frac{\boldsymbol{e}^{n+1}-\boldsymbol{e}^{n}}{\delta t}\|^2_{L^2(\Omega)^{d}}\leq C\delta t^4.$$

As for (3.31), using the previous estimates and stabilization results on the inhomogeneous Stokes problem [15], one can bound the error on q^{n+1} to obtain (3.21). This concludes the proof. □

The numerical stability of the divergence-free wavelet-based projection method was proved in [12], when using an implicit Euler time discretization scheme. For the two order time discretization schemes (2.4) and (2.5), we have:

THEOREM 3.3.
Suppose the initial condition $\boldsymbol{v}^0\in H^1_0(\Omega)^d$ and the source term $\boldsymbol{f}\in L^2(0,T,L^2(\Omega)^d)$. Then there exists a positive constant $C>0$ such that the numerical solution of (2.4) satisfies:

$$\forall\ n\geq 0,\quad \|\boldsymbol{v}^n\|_{L^2(\Omega)^d}+\|\nabla\boldsymbol{v}^n\|_{L^2(\Omega)^d}\leq C(\Omega,T,\nu,\boldsymbol{v}^0,\boldsymbol{f}). \quad (3.34)$$

Moreover, if $\boldsymbol{v}^1\in H^1_0(\Omega)^d$, the numerical solution of (2.5) satisfies:

$$\forall\ n\geq 0,\quad \|\boldsymbol{v}^n\|_{L^2(\Omega)^d}+\|\nabla\boldsymbol{v}^n\|_{L^2(\Omega)^d}\leq C(\Omega,T,\nu,\boldsymbol{v}^0,\boldsymbol{v}^1,\boldsymbol{f}). \quad (3.35)$$

Proof. The proof of (3.34) and (3.35) uses steps and tricks similar to those of Theorem 3.2: energy estimation, Poincaré and Young's inequalities. To avoid redundancy, we will summarize the most important steps in the case of the Gear scheme (2.5). Then, we start by pointing out that the first equation of (2.5) is very close to (3.7). To see this, it suffices to replace $\tilde{\boldsymbol{v}}^{n+1}$ by its expression $\tilde{\boldsymbol{v}}^{n+1}=\boldsymbol{v}^{n+1}+\nabla\Phi^{n+1}$ in (2.5):

$$\frac{3\boldsymbol{v}^{n+1}-4\boldsymbol{v}^{n}+\boldsymbol{v}^{n-1}}{2\delta t}-\nu\Delta\boldsymbol{v}^{n+1}+\nabla\left(\frac{3\Phi^{n+1}}{2\delta t}-\nu\Delta\Phi^{n+1}\right)=\boldsymbol{f}^{n+1}. \quad (3.36)$$

Due to the divergence-free property of $\boldsymbol{v}^{n+1}$ and the boundary conditions that it satisfies, integration by part with $4\delta t\boldsymbol{v}^{n+1}$ as the test function in (3.36) allows to get:

$$\|\boldsymbol{v}^{n+1}\|^2_{L^2(\Omega)^d} + \|2\boldsymbol{v}^{n+1} - \boldsymbol{v}^n\|^2_{L^2(\Omega)^d} - \|\boldsymbol{v}^n\|^2_{L^2(\Omega)^d} - \|2\boldsymbol{v}^n - \boldsymbol{v}^{n-1}\|^2_{L^2(\Omega)^d} + \|\boldsymbol{v}^{n+1} - 2\boldsymbol{v}^n + \boldsymbol{v}^{n-1}\|^2_{L^2(\Omega)^d} + 4\nu\delta t\|\nabla\boldsymbol{v}^{n+1}\|^2_{L^2(\Omega)^{d\times d}} \leq 4\delta t\|\boldsymbol{f}^{n+1}\|_{L^2(\Omega)^d}\|\boldsymbol{v}^{n+1}\|_{L^2(\Omega)^d}.$$

Then, using Poincaré and Young's inequalities and removing the positive term $\|\boldsymbol{v}^{n+1} - 2\boldsymbol{v}^n + \boldsymbol{v}^{n-1}\|^2_{L^2(\Omega)^d}$ and the viscous term $2\nu\delta t\|\nabla\boldsymbol{v}^{n+1}\|^2_{L^2(\Omega)^{d\times d}}$, we get:

$$\|\boldsymbol{v}^{n+1}\|^2_{L^2(\Omega)^d} + \|2\boldsymbol{v}^{n+1} - \boldsymbol{v}^n\|^2_{L^2(\Omega)^d} - \|\boldsymbol{v}^n\|^2_{L^2(\Omega)^d} - \|2\boldsymbol{v}^n - \boldsymbol{v}^{n-1}\|^2_{L^2(\Omega)^d} \leq \frac{C}{\nu}\delta t\|\boldsymbol{f}^{n+1}\|^2_{L^2(\Omega)^d}.$$

Making summation over n leads to:

$$\|\boldsymbol{v}^n\|^2_{L^2(\Omega)^d} + \|2\boldsymbol{v}^n - \boldsymbol{v}^{n-1}\|^2_{L^2(\Omega)^d} \leq \|\boldsymbol{v}^0\|^2_{L^2(\Omega)^d} + \|2\boldsymbol{v}^1 - \boldsymbol{v}^0\|^2_{L^2(\Omega)^d} + \frac{C}{\nu}\|\boldsymbol{f}\|^2_{L^2(0,T,L^2(\Omega)^d)} \quad (3.37)$$

Likewise, integration by part with $2(3\boldsymbol{v}^{n+1} - 4\boldsymbol{v}^n + \boldsymbol{v}^{n-1})$ as the test function in (3.36) gives:

$$\|\nabla\boldsymbol{v}^{n+1}\|^2_{L^2(\Omega)^{d\times d}} + \|\nabla(2\boldsymbol{v}^{n+1} - \boldsymbol{v}^n)\|^2_{L^2(\Omega)^{d\times d}} - \|\nabla\boldsymbol{v}^n\|^2_{L^2(\Omega)^{d\times d}} - \|\nabla(2\boldsymbol{v}^n - \boldsymbol{v}^{n-1})\|^2_{L^2(\Omega)^{d\times d}} \leq \frac{C}{\nu}\delta t\|\boldsymbol{f}^{n+1}\|^2_{L^2(\Omega)^d},$$

and by induction we also have:

$$\|\nabla\boldsymbol{v}^n\|^2_{L^2(\Omega)^{d\times d}} + \|\nabla(2\boldsymbol{v}^n - \boldsymbol{v}^{n-1})\|^2_{L^2(\Omega)^{d\times d}} \leq \|\nabla\boldsymbol{v}^0\|^2_{L^2(\Omega)^{d\times d}} + \|\nabla(2\boldsymbol{v}^1 - \boldsymbol{v}^0)\|^2_{L^2(\Omega)^{d\times d}} + \frac{C}{\nu}\|\boldsymbol{f}\|^2_{L^2(0,T,L^2(\Omega)^d)} \quad (3.38)$$

From (3.37) and (3.38), the second claim of the theorem is proved. □

The projection step in (2.4) and (2.5), involving the calculation of the Leray-Hopf projector $\mathbb{P}^{div,0}$, is executed by projecting onto the divergence-free basis. In practice, this is done by inverting the Gram matrix associated with this basis. Details of such a procedure are given in the next section.

4. Divergence-free wavelet basis Gram matrix inversion. To implement the proposed method, we employed the wavelet-based Galerkin method for spatial discretization [12]. The computation of the Leray-Hopf numerical projector, which involves projecting onto the divergence-free wavelet basis space, necessitates inverting the Gram matrix of the divergence-free wavelet basis. In this step, we opted for matrix diagonalization instead of the gradient descent algorithm used in [11, 12]. The procedure for the 2D and 3D wavelet bases is described below, and the generalization to higher dimensions is straightforward.

Consider $\Omega \subset \mathbb{R}^2$ to be the square $\Omega = [0,1]^2$, and let $\mathbf{V}_j^d = (V_j^d \otimes V_j^{0,d}) \times (V_j^{0,d} \otimes V_j^d)$ be a multiresolution analysis of $(H_0^1(\Omega))^2$ constructed from multiresolution analysis of $L^2(0,1)$ linked by differentiation and integration [11, 14], i.e.:

$$\frac{d}{dx}V_j^1 = V_j^0, \quad \text{with} \quad V_j^d = V_j^1 \cap H_0^1(0,1) \quad \text{and} \quad V_j^{0,d} = V_j^0 \cap H_0^1(0,1).$$

In this case, the wavelet $\psi^d_{j,k} = \psi^d(2^j. - k)$ associated with V^d_j also satisfies a differentiation relation:

$$(\psi^d_{j,k})' = 2^{j+2}(\psi^{0,d}_{j,k}),$$

where $\psi^{0,d}_{j,k}$ is the wavelet associated to $V^{0,d}_j$. See [11, 12, 14], a divergence-free wavelet basis for $\mathcal{H}_{div,0}(\Omega) = \{\boldsymbol{u} \in H^1_0(\Omega)^2 : \nabla \cdot \boldsymbol{u} = 0\} \subset \{\boldsymbol{u} = \mathbf{curl}(\Psi) : \Psi \in H^1_0(\Omega)\}$ is provided by taking the curl of scalar wavelets $\psi^d_{j_1,k_1} \otimes \psi^d_{j_2,k_2} \in H^1_0(\Omega)$:

$$\Psi^{div}_{\boldsymbol{j},\boldsymbol{k}} := \mathbf{curl}[\psi^d_{j_1,k_1} \otimes \psi^d_{j_2,k_2}] = \begin{pmatrix} \psi^d_{j_1,k_1} \otimes (\psi^d_{j_2,k_2})' \\ \\ -(\psi^d_{j_1,k_1})' \otimes \psi^d_{j_2,k_2} \end{pmatrix}.$$

Then, for $\boldsymbol{v}_j \in H^1_0(\Omega)^2$, its projection onto $\mathcal{H}_{div,0}(\Omega)$ is searched as:

$$\mathbb{P}^{div,0}(\boldsymbol{v}_j) = \sum_{|\boldsymbol{j}|<j,\boldsymbol{k}} d^{div}_{\boldsymbol{j},\boldsymbol{k}}\ \Psi^{div}_{\boldsymbol{j},\boldsymbol{k}},$$

where $\mathbb{P}^{div,0}$ denotes the Leray-Hopf projector. Thus, the computation of the wavelet coefficients $\left(d^{div}_{\boldsymbol{j},\boldsymbol{k}}\right)$ is performed by solving a linear system:

$$\mathbb{M}^{div}\left(d^{div}_{\boldsymbol{j},\boldsymbol{k}}\right) = \left(\langle \boldsymbol{v}_j, \Psi^{div}_{\boldsymbol{j},\boldsymbol{k}}\rangle\right), \tag{4.1}$$

where $\mathbb{M}^{div}$ denotes the Gram matrix of the divergence-free wavelet basis $\left\{\Psi^{div}_{\boldsymbol{j},\boldsymbol{k}}\right\}$. The elements of $\mathbb{M}^{div}$ are computed analytically by solving eigenvalue problems [2] and the computation of the right term $\langle \boldsymbol{v}_j, \Psi^{div}_{\boldsymbol{j},\boldsymbol{k}}\rangle$ of (4.1) is carried out using a quadrature formula, as explained in [10, 13]. Typically, to solve the system (4.1), iterative method is employed with an optimal diagonal preconditioner [11]. However, as mentioned earlier, we will exploit the tensor structure of the tensor structure of the basis to solve this system without using iterations. Specifically, let's define the mass and stiffness matrices of the one-dimensional wavelet basis:

$$\mathcal{M}^d = [\langle \psi^d_{j,k}, \psi^d_{j',k'}\rangle],\ \mathcal{R}^d = [\langle (\psi^d_{j,k})', (\psi^d_{j',k'})'\rangle] \text{ and } \mathcal{A}^0_d = [\langle \psi^{0,d}_{j,k}, (\psi^d_{j',k'})'\rangle].$$

Then, in terms of matrix equation, the system (4.1) is rewritten:

$$\mathcal{M}^d\ [d^{div}_{\boldsymbol{j},\boldsymbol{k}}]\ \mathcal{R}^d + \mathcal{R}^d\ [d^{div}_{\boldsymbol{j},\boldsymbol{k}}]\ \mathcal{M}^d = \mathcal{M}^d\ [d^1_{\boldsymbol{j},\boldsymbol{k}}]\ \mathcal{A}^0_d - (\mathcal{A}^0_d)^T\ [d^2_{\boldsymbol{j},\boldsymbol{k}}]\ \mathcal{M}^d, \tag{4.2}$$

where $d^1_{\boldsymbol{j},\boldsymbol{k}}$ and $d^2_{\boldsymbol{j},\boldsymbol{k}}$ represent the wavelet coefficients of the projection of $\boldsymbol{v}_j = (v_{1,j}, v_{2,j})$ onto the wavelet basis of $\mathbf{V}^d_j$:

$$v_{1,j} = \sum_{|\boldsymbol{j}|<j,\boldsymbol{k}} d^1_{\boldsymbol{j},\boldsymbol{k}}\ \psi^d_{j_1,k_1} \otimes \psi^{0,d}_{j_2,k_2} \text{ and } v_{2,j} = \sum_{|\boldsymbol{j}|<j,\boldsymbol{k}} d^2_{\boldsymbol{j},\boldsymbol{k}}\ \psi^{0,d}_{j_1,k_1} \otimes \psi^d_{j_2,k_2}. \tag{4.3}$$

Since the matrix $\mathcal{M}^d$ is symmetric, positive and definite, we define $\mathcal{M} = (\mathcal{M}^d)^{-1}\mathcal{R}^d$, allowing us to rewrite the system (4.2) as:

$$[d^{div}_{\boldsymbol{j},\boldsymbol{k}}]\ \mathcal{M}^T + \mathcal{M}\ [d^{div}_{\boldsymbol{j},\boldsymbol{k}}] = [b_{\boldsymbol{j},\boldsymbol{k}}], \tag{4.4}$$

with

$$[b_{\boldsymbol{j},\boldsymbol{k}}] = [d^1_{\boldsymbol{j},\boldsymbol{k}}]\ \mathcal{A}^0_d(\mathcal{M}^d)^{-1} - (\mathcal{M}^d)^{-1}(\mathcal{A}^0_d)^T\ [d^2_{\boldsymbol{j},\boldsymbol{k}}]. \tag{4.5}$$

Upon diagonalizing the matrix $\mathcal{M}$ as $\mathcal{M} = \mathcal{U}\mathcal{D}\mathcal{U}^{-1}$, the system (4.4) becomes:

$$[d^{div}_{\boldsymbol{j},\boldsymbol{k}}]\ \mathcal{U}^T\mathcal{D}\mathcal{U}^{-T} + \mathcal{U}\mathcal{D}\mathcal{U}^{-1}\ [d^{div}_{\boldsymbol{j},\boldsymbol{k}}] = [b_{\boldsymbol{j},\boldsymbol{k}}],\ \text{with}\ \mathcal{M} = \mathcal{U}\mathcal{D}\mathcal{U}^{-1}. \tag{4.6}$$

This still becomes:

$$[\bar{d}^{div}_{\boldsymbol{j},\boldsymbol{k}}]\mathcal{D} + \mathcal{D}[\bar{d}^{div}_{\boldsymbol{j},\boldsymbol{k}}] = [\bar{b}_{\boldsymbol{j},\boldsymbol{k}}], \tag{4.7}$$

where

$$[\bar{d}^{div}_{\boldsymbol{j},\boldsymbol{k}}] = \mathcal{U}^{-1}[d^{div}_{\boldsymbol{j},\boldsymbol{k}}]\mathcal{U}^T \quad \text{and} \quad [\bar{b}_{\boldsymbol{j},\boldsymbol{k}}] = \mathcal{U}^{-1}[b_{\boldsymbol{j},\boldsymbol{k}}]\mathcal{U}^T.$$

By performing element-wise matrix division in (4.7), the coefficients $[\bar{d}^{div}_{\boldsymbol{j},\boldsymbol{k}}]$ are obtained as:

$$[\bar{d}^{div}_{\boldsymbol{j},\boldsymbol{k}}]_{m,n} = [\bar{b}_{\boldsymbol{j},\boldsymbol{k}}]_{m,n} / \left(\mathcal{D}_{n,n} + \mathcal{D}_{m,m}\right). \tag{4.8}$$

As the matrices $\mathcal{M}^d$ and $\mathcal{R}^d$ are symmetric and positive definite, we always have:

$$\mathcal{D}_{n,n} + \mathcal{D}_{m,m} > 0, \quad \forall\ n,\ m.$$

This is a consequence of the well-known property of symmetric positive definite matrices. Specifically, if A and B are two symmetric positive definite matrices, then AB and BA share the same eigenvalues. Thus, taking $U = BA^{1/2}$ and $P = A^{1/2}$, the same argument demonstrates that UP and PU have the same eigenvalues. By definition, PU is a symmetric positive definite matrix. Therefore, the denominator in (4.8) cannot vanish.

The method for resolving the system (4.4) easily extends to higher dimensions. Similarly, we only need to diagonalize the Gram matrix of the one-dimensional wavelet basis. For instance, in the case of three-dimensional space, defining $[\bar{d}^{div}\boldsymbol{j},\boldsymbol{k}] = (\mathcal{U}^{-1}\otimes \mathcal{U}\otimes\mathcal{U})[d^{div}\boldsymbol{j},\boldsymbol{k}]$, the array system analogous to (4.7) is:

$$\left(\mathcal{I}\otimes\mathcal{I}\otimes\mathcal{D} + \mathcal{I}\otimes\mathcal{I}\otimes\mathcal{D} + \mathcal{D}\otimes\mathcal{I}\otimes\mathcal{I}\right)[\bar{d}^{div}_{\boldsymbol{j},\boldsymbol{k}}] = [\bar{b}_{\boldsymbol{j},\boldsymbol{k}}], \tag{4.9}$$

where $\mathcal{I}$ is the identity matrix. Then, the coefficients $[\bar{d}^{div}_{\boldsymbol{j},\boldsymbol{k}}]$ are given by:

$$[\bar{d}^{div}_{\boldsymbol{j},\boldsymbol{k}}]_{m,n,l} = [\bar{b}_{\boldsymbol{j},\boldsymbol{k}}]_{m,n,l} / \left(\mathcal{D}_{n,n} + \mathcal{D}_{m,m} + \mathcal{D}_{l,l}\right). \tag{4.10}$$

It is worth noting that, except for the diagonalization of the Gram matrix of the one-dimensional basis, the numerical cost of this approach is approximately $\mathcal{O}(N)$, and its efficiency is tested in the next section.

5. Numerical results. This section presents numerical results to verify the error estimates of Theorem 3.2 and evaluate the efficiency of the projection step outlined in Section 4. Initially, we assess the computational cost of the projection step when matrix diagonalization is employed instead of a conjugate gradient algorithm [11] to solve system (4.1). Subsequently, using manufactured solutions, we conduct numerical simulations that confirm the convergence rate of schemes (2.4) and (2.5) is indeed second-order for the time discretization error.

To measure the CPU time of the projection step and assess its efficiency, we employed the initial condition of the Taylor-Green vortex in two spatial dimensions as the analytical solution:

$$\begin{aligned} \boldsymbol{v}(x,y,t) &= e^{-2\mu t}\left(-\sin(2\pi x)\cos(2\pi y); \cos(2\pi x)\sin(2\pi y)\right), \\ p(x,y,t) &= \frac{1}{4\pi} e^{-4\mu t}\left(\sin(2\pi x) + \cos(2\pi y)\right). \end{aligned} \tag{5.1}$$

The Taylor-Green vortex represents an unsteady flow of a decaying vortex, and it shares the same closed-form solution as the incompressible Navier-Stokes equations in Cartesian coordinates.

For the all experiment, the spatial computational domain is the square $\Omega = [0,1]^2$ and we used the Daubechies orthogonal wavelet generator ψ^1 with $r = 4$ vanishing moments to construct the multi-resolution analysis linked by differentiation/integration necessary to construct the divergence-free wavelet basis [11, 14]. Table 5.1 shows the computational time of the MATLAB code executed on a MacBook Pro 15 (2.6 GHz, 4-core Intel Core i7 processor and 16 Go LPDDR3 SDRAM). We find that the proposed method, when using matrix diagonalisation to solve (4.1), speeds up the projection step by about five times. However, we note that the execution speed of the MATLAB code depends on its optimisation, MATLAB prefers vectorized codes. Therefore, these results should be analyzed carefully. Table 5.2 shows the L^2 errors computed at grid points. Again, the proposed method performs better than a conjugate gradient method, but the error increases slightly as the spatial resolution increases. We think that, it is due to the diagonalisation algorithm, which loses accuracy for large matrices.

Space resolution j	7	8	9	10
CG method	0.07999	0.32999	1.31000	8.45000
Proposed method	0.02999	0.07000	0.25000	1.36999
Improvement rate	2.6672	4.71414	5.240000	6.16792

TABLE 5.1
CPU time in second for the projection step in 2D.

The performance of the proposed schemes (2.4) and (2.5) was firstly examined under periodic boundary conditions. Utilizing (5.1) as the exact Navier-Stokes solution, the source term is calculated such that $\mathbf{f} = \partial_t \mathbf{v} - \nu\Delta\mathbf{v} + (\mathbf{v}\cdot\nabla)\mathbf{v} + \nabla p$, where the viscosity is set to $\nu = 0.01$. The simulation duration is fixed at $T = 1$, and we varied

Space resolution j	7	8	9	10
L^2-error-CG method	4.9357E-08	1.2532E-08	1.2104E-08	7.2741E-09
L^2-error-**Proposed method**	6.6506E-12	2.6312E-11	1.0660E-10	4.1975E-10

TABLE 5.2
L^2-error $\|\boldsymbol{v} - \mathbb{P}(\boldsymbol{v})\|_{L^2}$ of the divergence-fee projection of solution (5.1).

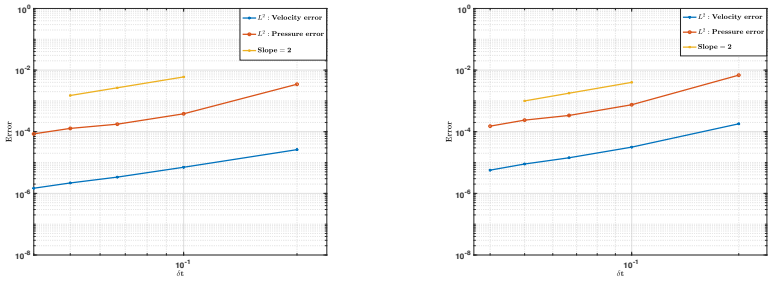

(a) (b)

FIGURE 5.1. *Plot of the L^2-norm of the errors $|\boldsymbol{v}(.,1) - v^N(.)|$ and $|p(.,1) - p^N(.)|$, according to the time step δt in loglog scale. For the exact solution $(\boldsymbol{v}, p)$ defined in* (5.1) *and final time $T = 1 = N\delta t$: Crank-Nicholson scheme (left) and Gear scheme (right), where ψ^1 is the Daubechies orthogonal wavelet generator with $r = 4$ vanishing moments.*

the time step δt in line with the usual CFL condition to study temporal discretization rate and accuracy. At each iteration, the non-linear term is computed at grid points using a fourth-order finite difference method with $\delta x = \delta y = 2^{-j}$ per direction. We recall that $r = 4$ represents the maximum order of polynomial reproduction of the scaling function associated with ψ^1.

For the Crank-Nicholson scheme (2.2), the term $(\mathbf{v} \cdot \nabla)\mathbf{v}$ is approximated in time by a two-order Adams-Bashforth scheme:

$$\frac{1}{2}[(\boldsymbol{v}^{n+1} \cdot \nabla)\boldsymbol{v}^{n+1} + \boldsymbol{v}^n \cdot \nabla)\boldsymbol{v}^n] \approx \frac{3}{2}(\boldsymbol{v}^n \cdot \nabla)\boldsymbol{v}^n - \frac{1}{2}\boldsymbol{v}^{n-1} \cdot \nabla)\boldsymbol{v}^{n-1},$$

and we used a two-order extrapolation scheme for the Gear system (2.3):

$$(\boldsymbol{v}^{n+1} \cdot \nabla)\boldsymbol{v}^{n+1} \approx 2(\boldsymbol{v}^n \cdot \nabla)\boldsymbol{v}^n - (\boldsymbol{v}^{n-1} \cdot \nabla)\boldsymbol{v}^{n-1}.$$

Figure 5.1 displays the L^2-errors on the numerical solutions computed with schemes (2.4) and (2.5). The numerical pressures $\bar{p}^{n+1/2}$ and $\bar{p}^{n+1}$ are computed by solving Poisson equations where the source term corresponds to the divergence of equation (2.9) and (2.10), respectively. For the two schemes, as observed in Figure 5.1, the expected time discretization convergence rate in $\mathcal{O}(\delta t^2)$, is achieved in both velocity and pressure approximation. This confirms the theoretical error estimates of Theorem 3.2.

In the cas of homogeneous Dirichlet boundary conditions, as exact solution of (2.1) we took:

$$\begin{aligned} \boldsymbol{v}(x, y, t) &= 2\pi \sin(t) \left(\sin^2(2\pi x)\sin(4\pi y); -\sin(4\pi x)\sin^2(2\pi y)\right). \\ p(x, y, t) &= \sin(t)\cos(2\pi x)\sin(2\pi y). \end{aligned} \tag{5.2}$$

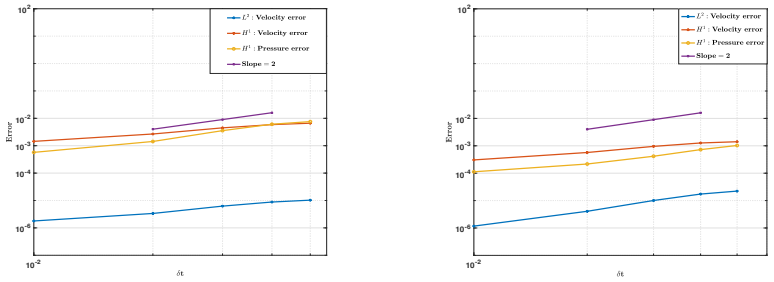

(a) (b)

FIGURE 5.2. *L^2-norm and H^1-norm of the errors $|\boldsymbol{v}(.,1) - v^N(.)|$ and $|p(.,1) - p^N(.)|$ for $(\boldsymbol{v}, p)$ defined in* (5.2) *and $N\delta t = T = 1$ is the final time: Crank-Nicholson scheme (left) and Gear scheme (right), where ψ^1 is the Daubechies orthogonal generator with $r = 4$ vanishing moments.*

Similarly, a source term $\mathbf{f}$ is added with viscosity $\nu = 0.0001$. The nonlinear term is still computed using a fourth-order finite difference method at grid points. For the solution (5.2), we are unable to compare the L^2-error on the pressure directly. Typically, to obtain $\bar{p}^{n+1/2}$ and $\bar{p}^{n+1}$, in the common approaches, an artificial boundary condition is imposed in (2.9) and (2.10), which is not the case in our method. Therefore, we compare the norm of the pressure gradient according to the time step δt and in log-log scale, Figure 5.2 shows the plot of the L^2-norm and H^1-norm of the error on the velocity, as well as the L^2-norm of the error on the pressure gradient. Similar to the periodic case, the dominant part of the curve has a slope $s = 2$, indicating that the optimal convergence rate $\mathcal{O}(\delta t^2)$ is achieved.

6. Conclusion. We studied the order and the convergence rate of the velocity and the pressure time discretization in the case of the divergence-free wavelet based projection method for viscous fluid. Second-order numerical schemes have been studied and it has been shown that the optimal order $\mathcal{O}(\delta t^2)$ is reached, particularly on the pressure and the velocity gradient approximation. This is not the case for example with classical methods, where the splitting error does not allow for optimal convergence. We have also shown that the use of matrix diagonalization speeds up the algorithm of the projection onto the divergence-free wavelet basis and all this has been verified and documented by numerical experiments. Since the method can be interpreted as a change of variables and the projection step does not required the pressure, we believe that the use of high order schemes (more than two), for the time discretization, does not reduce the accuracy of the method. This question is one of the subject we'll be exploring next.

REFERENCES

[1] P. ANGOT, R. CHEAYTOU, *On the error estimates of the vector penalty-projection methods: Second-order scheme*, Math. Comp., 87 (2018), pp. 2159–2187.

[2] G. BEYLKIN, *On the representation of operator in bases of compactly supported wavelets*, SIAM J. Numer. Anal., 6 (1992), pp. 1716–1740.

[3] D. Boffi, F. Brezzi, M. Fortin, *Mixed finite element methods and applications*, Volume 44, Springer Series in Computational Mathematics, (2013).

[4] A.J. CHORIN, *Numerical simulation of the Navier-Stokes equation*, Math. Comp., 22 (1968), pp. 745–762.

[5] W. E, J. Guo-Liu , *Projection Method I: Convergence and Numerical Boundary Layers*, SIAM J. Numer. Anal., 32 (1995), pp. 1017–1057.
[6] V. Girault, P.A. Raviart, *Finite element methods for Navier-Stokes equations*, Springer-Verlag Berlin, (1986).
[7] J.-L. Guermond, P. Minev, *High-order Time Stepping for the Incompressible Navier-Stokes equations*, SIAM J. Sci. Comput., **37(6)** (2015) A2656–A2681.
[8] J.-L. Guermond, P. Minev, J. Shen, *An Overview of Projection methods for incompressible flows*, Computer Methods in Applied Mechanics and Engineering, **195** (2006) 6011–6045.
[9] J. Kim, P. Moin, *Application of a fractional-step method to incompressible Navier-Stokes equations*, J. Comp. Phys., 59 (1985), pp. 308–323.
[10] S. Kadri-Harouna, V. Perrier, *Helmholtz-Hodge Decomposition on* $[0,1]^d$ *by Divergence-free and Curl-free Wavelets*, Curves and Surfaces, proc of the 7th International Conference, Avignon, France, June 24-30, 2010, Boissonnat, J.-D.; Chenin, P.; Cohen, A.; Gout, C.; Lyche, T.; Mazure, M.-L.; Schumaker, L. (Eds.), Lecture Notes in Computer Science series, 6920, Springer (2012), pp. 311–329.
[11] S. Kadri-Harouna, V. Perrier, Effective construction of divergence-free wavelets on the square, *J. of Computational and Applied Math.* **240** (2013) 74–86.
[12] S. Kadri-Harouna, V. Perrier, Divergence-free Wavelet Projection Method for Incompressible Viscous Flow, *SIAM Multiscale Modeling and Simulation* **13(1)** (2015) 399–422.
[13] P. Monasse, V. Perrier, *Orthogonal Wavelet Bases Adapted For Partial Differential Equations With Boundary Conditions*, SIAM J. Math. Anal., 29 (1998), pp. 1040–1065.
[14] R. Stevenson, Divergence-free wavelets on the hypercube: general boundary conditions, *Constr. Approx.*, **44(2)** (2016), 233–267.
[15] R. Temam, *Navier Stokes Equations, North Holland*, New York, 1977.
[16] C. Wang, J-G. Liu, *Convergence of Gauge method for incompressible flow*, Math. Comput., 69 (2000), pp. 1385–1407.